54. T.J. O'Kane and J.S. Frederiksen, A comparison of statistical dynamical and ensemble prediction during blocking, *submitted.*
55. T.J. O'Kane and J.S. Frederiksen, Comparison of statistical dynamical, square root and ensemble Kalman filters, *submitted.*
56. S.A. Orszag, Analytical theories of turbulence *J. Fluid Mech.* **41**, 363–386 (1970).
57. D.F. Parish and J.C. Derber, The national meteorological center's spectral statistical-interpolation analysis system *Mon. Wea. Rev.* **120**, 1747–1763 (1992).
58. E.J. Pitcher, Application of stochastic dynamic prediction to real data *J. Atmos. Sci.* **34**, 3–21 (1977).
59. I. Proudman and W.H. Reid, On the decay of a normally distributed and homogeneous turbulent vector field *Philosophical transactions of the Royal Society of London. Ser. A* **247**, 163–189 (1954).
60. F. Rabier, A. McNally, E. Andersson, P. Courtier, P. Undén, J. Eyre, A. Hollingsworth and F. Bouttier, The ECMWF implementation of three-dimensional variational assimilation (3D-Var). II: Structure functions *Q. J. R. Meteorol. Soc.* **124**, 1809–1829 (1998).
61. H.A. Rose, An efficient non-Markovian theory of non-equilibrium dynamics *Physica D* **14**, 216–226 (1985).
62. P. Sakov, P.R. Oke and S.P. Corney, On the form of the ensemble transformation matrix in ensemble square root filters *submitted Mon. Wea. Rev.* (2006).
63. J. Smagorinsky, Problems and promises of deterministic extended range forecasting *Bull. Amer. Meteor. Soc.* **50**, 286–311 (1969).
64. M.K. Tippett, J.L. Anderson, C.H. Bishop, T.M. Hamill and J.S. Whitaker, Ensemble square root filters *Mon. Wea. Rev.* **131**, 1485–1490 (2003)
65. Z. Toth and E. Kalnay, Ensemble forecasting at NMC: The generation of perturbations *Bull. Amer. Meteor. Soc.* **74**, 2317–2330 (1993).
66. Z. Toth and E. Kalnay, Ensemble forecasting at NMC: The use of the breeding method for generating perturbations *Proc. Tenth Conference on Numerical Weather Prediction, 1994.* Portland.
67. Z. Toth and E. Kalnay, Ensemble forecasting at NCEP and the breeding method *Mon. Wea. Rev.* **125**, 3297–3319 (1997).
68. P. Veyre, Direct prediction of error variances by the tangent linear model: A way to forecast uncertainty in the short range? *New developments in predictability; Proceedings of a workshop held at ECMWF*, Reading U.K., 65–86 (1991).
69. X. Wang and C.H. Bishop, A comparison of breeding and ensemble transform Kalman filter ensemble forecast schemes *J. Atmos. Sci.* **60**, 1140–1158 (2003).
70. J.S. Whitaker and T.M. Hamill, Ensemble data assimilation without perturbed observations *Mon. Wea. Rev.* **130**, 1913–1924 (2002).

DISTILLED TURBULENCE. A REDUCED MODEL FOR CONFINEMENT TRANSITIONS IN MAGNETIC FUSION PLASMAS

ROWENA BALL

Mathematical Sciences Institute and Department of Theoretical Physics
The Australian National University, Canberra ACT 0200 Australia,
Rowena.Ball@anu.edu.au

Two different views of the physics behind plasma confinement transitions are unified in a reduced, or distilled, model for the coupled dynamics of potential, turbulence, and shear flow energy subsystems. A regime of super-suppressed turbulence is shown to occur at low power input.

1. Introduction

Imagine a fractional distillation column for which the feedstock is not crude oil but a flow of high purity and Reynolds number. Then the feedstock is not some natural distribution over hydrocarbon molecular weights but an energy distribution over scales of motion. We know, in principle, how hydrocarbons are separated in the still according to their boiling points (even if we do not work at an oil refinery), but how do we separate and re-form the energy components of the pure turbulent fluid? And why should we do this anyway?

First, our turbulence refinery does not define the skyline of a seamy port city in complicated chiaroscuro, but exists only inside the computer. And computation is, in essence, the notorious "problem of turbulence". In a turbulent flow energy is distributed over wavenumbers that range over perhaps seven orders of magnitude (for, say, a tokamak) to twelve orders of magnitude (for a really huge system, say a supernova). To simulate a turbulent flow in the computer it is necessary to resolve all relevant scales of motion in three dimensions. As pointed out recently[1] such calculations would take 400 years at today's processor speeds, therefore a faster way to do them would be to rely on Moore's law and wait only 20 years until computers are speedy enough. While we are waiting, we can study various classes of reduced, or distilled, dynamical models for turbulent systems:

(1) Metaphors, e.g., predator-prey models.
(2) Fourier mode truncations, e.g., the Lorenz equations.
(3) Spatial averages with semi-empirical closures.
(4) Mixed metaphors, or elements of all of the above.

For this workshop I describe an application of class 3, in which the components of the global dynamics are distilled rather than the motions on individual spatial scales.

2. Two-dimensional turbulence in plasmas

Magnetized fusion plasmas are strongly driven dissipative flows in which the kinetic energy of small-scale turbulence can drive the formation of large-scale coherent structures such as sheared mass flows. This tendency to self-organise is typical of flows where Lagrangian fluid elements see globally prevalent or soliton-like two-dimensional velocity fields, and is a consequence of non-negligible inverse energy cascades.[2]

The distinctive properties of quasi two-dimensional fluid motion are the basis of natural phenomena such as zonal structuring of planetary flows and the segregation of pebbles washed by the sea on a beach (Fig. 1), but are under-exploited in technologies. The propensity of two-dimensional flows to structure themselves — and hence organise any advected or diffusively transported particles or heat — is a fair prospect for achieving directed management of turbulent transport in industrial flows, but it is only in fusion plasmas that this potential has been realized to some extent.

In fusion devices the most useful consequence of two-dimensional fluid motion is a dramatic enhancement of sheared mass flows concomitant with suppression of the high wavenumber turbulence at the edge that degrades confinement.[3] These low- to high-confinement (L–H) transitions have been investigated intensively since the 1980s. Two major strands in the literature emerged early and are supported by experiments: (1) They are an internal phenomenon that occurs spontaneously when upscale energy transfer from turbulence to shear flows exceeds nonlinear dissipation;[4,5] (2) They are due to edge ion orbit losses or induced biasing, the resulting electric field providing a torque which drives shear flows nonlinearly.[6–8]

In this contribution I give a condensed account of how these two different strands may be unified in a reduced dynamical model, the essence of which is distilled from MHD equations using technique (3). The model is developed and strengthened by interrogating degenerate singularities and matching

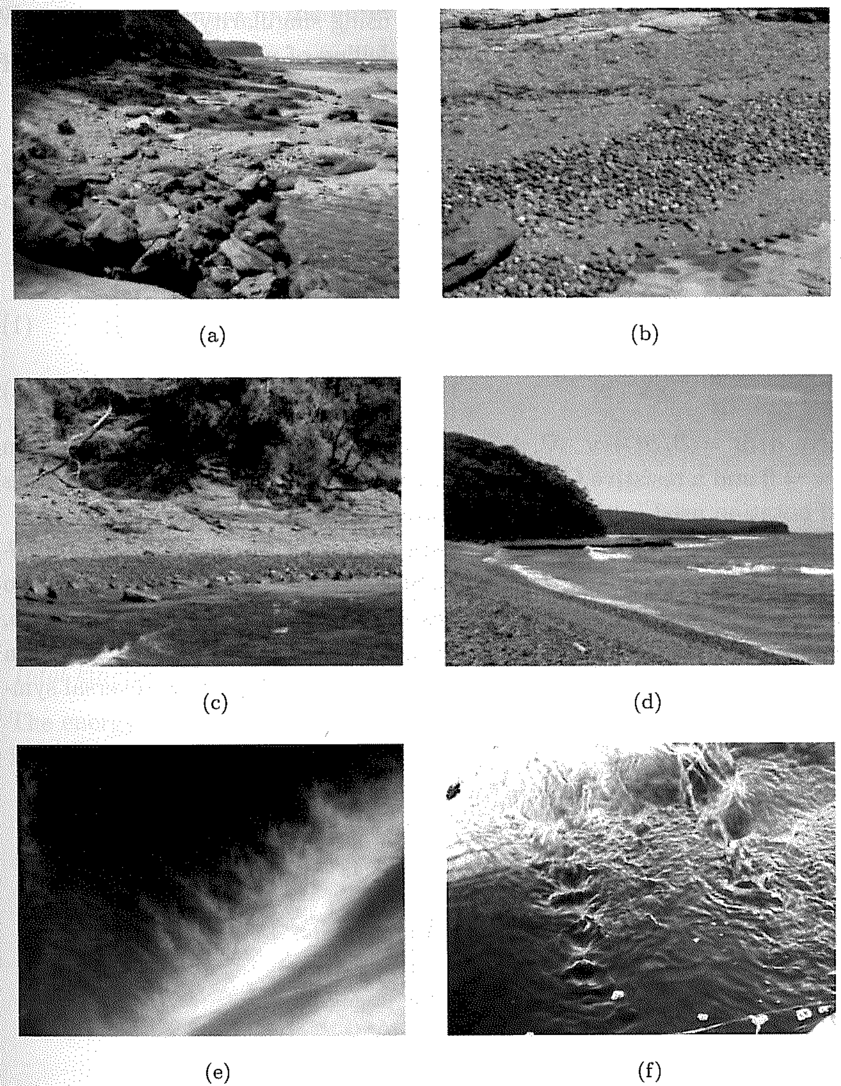

Fig. 1. (a) – (d) On Pebbly Beach, NSW, the sea has sorted and segregated the stones according to size. (e) A rare cloud over Canberra. Secondary instabilities grow from the edge of this streaming cloud formation, a fast-moving zonal flow. (f) Sullivans Creek, Canberra. Kinetic energy seems to cascade from both turbulent and laminar flow regions into coherent structures. (Photos by the author.)

their unfoldings to appropriate physics, using singularity theory methods[9] that were first applied to dynamical modelling of magnetic fusion plasmas by Ball and Dewar.[10]

3. Recipe for the reduced model

Take the following MHD momentum and pressure convection equations:

$$\rho \frac{\mathrm{d}\mathbf{v}}{\mathrm{d}t} = -\nabla p + \mathbf{J}\times\mathbf{B} + \mu\nabla_\perp^2 \mathbf{v} + \Omega' \tilde{p}\hat{x} - \rho\nu\left(\mathbf{v} - V(x)\,\hat{y}\right) \tag{1}$$

$$\frac{\mathrm{d}p}{\mathrm{d}t} = \chi\nabla_\perp^2 p, \tag{2}$$

where $\mathrm{d}/\mathrm{d}t = \partial/\partial t + \mathbf{v}\cdot\nabla$, together with an incompressibility condition $\nabla\cdot\mathbf{v} = 0$ and a resistive Ohm's law $\mathbf{E} + \mathbf{v}\times\mathbf{B} = \eta\mathbf{J}$. A guide to the symbols and notation used in this section is provided in the table at the end.

Equations 1 and 2 are the electrostatic limit of the reduced MHD equations that were originally derived by Strauss.[11] They have been shown to describe well the nonlinear dynamics of a high beta, large aspect ratio, tokamak plasma.[12–15] Here an additional term $\rho\nu\left(\mathbf{v} - V(x)\,\hat{y}\right)$ has been included in the momentum balance, which breaks shear flow reversal symmetry.

Put them in slab geometry:

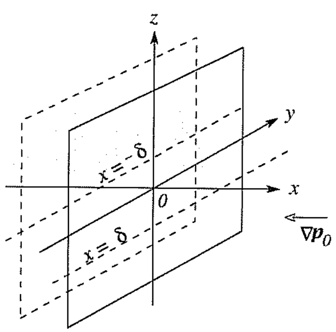

Fig. 2. The plasma edge region is $-\delta < x < \delta$, with $x = \delta$ at the plasma surface. $\nabla p_0 < 0$ is the y,z-averaged pressure gradient. $\langle\cdot\rangle$ denotes the average over the (y,z) plane.

Extract the dynamics of the mean flow:

From Eq. 1 averaged over the (y,z) plane we obtain

$$\partial_t v_0 - \mu\partial_x^2 v_0 + \partial_x\langle\tilde{v}_x\tilde{v}_y\rangle = -\nu(v_0 - V),$$

where $v_0 = \langle v_y\rangle$, $\mathbf{v} == \mathbf{v}_0 + \tilde{\mathbf{v}}$. We multiply by v_0 and integrate over x to obtain the evolution of the background shear flow kinetic energy F:

$$\frac{\mathrm{d}}{\mathrm{d}t}\left[\frac{1}{\delta}\int_{-\delta}^{\delta}\frac{\mathrm{d}x}{2}\,v_0^2\right] = -\frac{1}{\delta}\int_{-\delta}^{\delta}\mathrm{d}x\,\left[\mu\left(\frac{\mathrm{d}v_0}{\mathrm{d}x}\right)^2 + \nu\,v_0^2\right] + \frac{1}{\delta}\int_{-\delta}^{\delta}\mathrm{d}x\,\langle\tilde{v}_x\tilde{v}_y\rangle\frac{\mathrm{d}v_0}{\mathrm{d}x} + \frac{1}{\delta}\int_{-\delta}^{\delta}\mathrm{d}x\,\nu V v_0,$$

which we re-write as

$$\frac{\mathrm{d}}{\mathrm{d}t}F = -\epsilon_F + E_F + E_\varphi,$$

where $F \equiv \frac{1}{\delta}\int_{-\delta}^{\delta}\frac{\mathrm{d}x}{2}\,v_0^2$, $\epsilon_F \equiv \frac{1}{\delta}\int_{-\delta}^{\delta}\mathrm{d}x\,\left[\mu\left(\frac{\mathrm{d}v_0}{\mathrm{d}x}\right)^2 + \nu\,v_0^2\right]$, $E_F \equiv \frac{1}{\delta}\int_{-\delta}^{\delta}\mathrm{d}x\,\langle\tilde{v}_x\tilde{v}_y\rangle\frac{\mathrm{d}v_0}{\mathrm{d}x}$, and $E_\varphi \equiv \frac{1}{\delta}\int_{-\delta}^{\delta}\mathrm{d}x\,\nu V v_0$.

Total kinetic energy:

The energy moment of Eq. 1 gives the dynamics of the background shear flow plus fluctuation kinetic energy.

$$\frac{\mathrm{d}}{\mathrm{d}t}\left[\frac{1}{\delta}\int_{-\delta}^{\delta}\frac{\mathrm{d}x}{2}\,(v_0^2 + \tilde{v}^2)\right] = \frac{1}{\delta}\int_{-\delta}^{\delta}\mathrm{d}x\,\Omega'\frac{\langle\tilde{p}\,\tilde{v}_x\rangle}{\rho} - \frac{1}{\delta}\int_{-\delta}^{\delta}\mathrm{d}x\,\left[\frac{\eta}{\rho_m}\left\langle\tilde{J}_\parallel^2\right\rangle + \mu\left\langle\left(\frac{\partial\tilde{v}_i}{\partial x_j}\right)^2\right\rangle\right] - \frac{1}{\delta}\int_{-\delta}^{\delta}\mathrm{d}x\,\left[\mu\left(\frac{\mathrm{d}v_0}{\mathrm{d}x}\right)^2 + \nu\,v_0^2\right] + \frac{1}{\delta}\int_{-\delta}^{\delta}\mathrm{d}x\,\nu V v_0,$$

which we re-write as

$$\frac{\mathrm{d}}{\mathrm{d}t}[F + N] = E_N - \epsilon_N - \epsilon_F + E_\varphi,$$

where $N \equiv \frac{1}{\delta}\int_{-\delta}^{\delta}\frac{\mathrm{d}x}{2}\,\tilde{v}^2$, $E_N \equiv \frac{1}{\delta}\int_{-\delta}^{\delta}\mathrm{d}x\,\Omega'\frac{\langle\tilde{p}\,\tilde{v}_x\rangle}{\rho}$ and $\epsilon_N \equiv \frac{1}{\delta}\int_{-\delta}^{\delta}\mathrm{d}x\,\left[\frac{\eta}{\rho_m}\left\langle\tilde{J}_\parallel^2\right\rangle + \mu\left\langle\left(\frac{\partial\tilde{v}_i}{\partial x_j}\right)^2\right\rangle\right]$.

Potential energy dynamics:

We assume the cross-field thermal diffusivity can be neglected and obtain the evolution of potential energy in the pressure gradient as:

$$\frac{\mathrm{d}}{\mathrm{d}t}\left[\frac{1}{\delta}\int_{-\delta}^{\delta}\mathrm{d}x\ (-x)\,\Omega'\frac{p_0}{\rho}\right] = \frac{\langle\tilde{p}\tilde{v}_x\rangle|_{-\delta}^{\delta}}{\rho}\Omega' - \frac{1}{\delta}\int_{-\delta}^{\delta}\mathrm{d}x\ \frac{\langle\tilde{p}\tilde{v}_x\rangle}{\rho}\Omega',$$

which we re-write as

$$\varepsilon\frac{\mathrm{d}}{\mathrm{d}t}P = E_P - E_N, \qquad P \equiv \frac{1}{\delta}\int_{-\delta}^{\delta}\mathrm{d}x\ (-x)\,\Omega' p_0/\rho,$$

where $\varepsilon P \equiv \frac{1}{\delta}\int_{-\delta}^{\delta}\mathrm{d}x\ (-x)\,\Omega' p_0/\rho$, ε is the specific heat capacity, and $E_P \equiv \frac{\langle\tilde{p}\tilde{v}_x\rangle|_{-\delta}^{\delta}}{\rho}\Omega'$.

Closure and approximations:

We need explicit expressions for the averaged rates of energy input, transfer, and loss on the right hand sides. In general, such averaged rate laws for mass or energy conversions cannot be derived from theory but must be postulated using physical arguments and tested by experiments. We make use of the approximations and definitions given in the table at the end to obtain the closed dynamical system,

$$\varepsilon\frac{\mathrm{d}P}{\mathrm{d}t} = Q - \gamma NP \tag{10}$$

$$\frac{\mathrm{d}N}{\mathrm{d}t} = \gamma NP - \alpha v'^2 N - \beta N^2 \tag{11}$$

$$2\frac{\mathrm{d}v'}{\mathrm{d}t} = \alpha v' N - \mu(P,N)v' + \varphi. \tag{12}$$

The easy way:

A schematic showing the energy fluxes through the P, N, and v' subsystems is shown in Fig. 3(a). The skeleton dynamical system can be written down directly from the schematic by inspection, and fleshed out using the approximations and definitions given in the table.

4. Analysis of and modifications to the distilled model

In this work the terms *bifurcation structure* or *bifurcation analysis* refer collectively to the stability and singularity analysis of equilibria and periodic

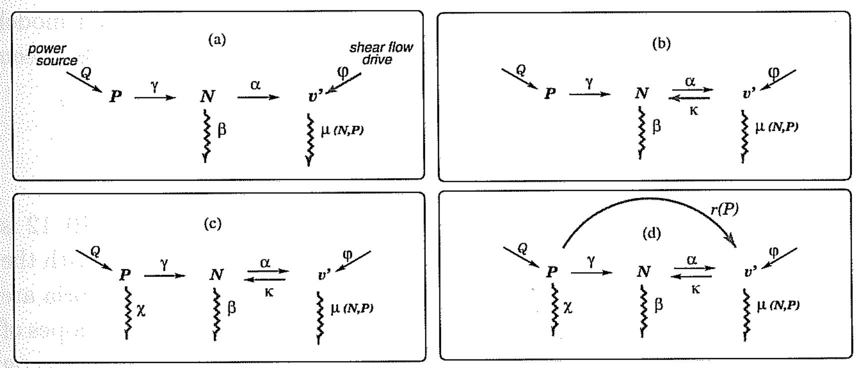

Fig. 3. Energy flux schematics through the potential energy P, turbulent kinetic energy N, and shear flow v' subsystems. See text for explanations of each subfigure. Curly arrows indicate dissipative channels, straight arrows indicate inputs and transfers between energetic subsystems.

solutions *and* assessment of the structural stability of a dynamical system. The principles of stability theory are well-known; singularity theory less so. A brief exposition is given in the Appendix. Singularity theory is a systematic methodology for characterizing the equilibria of dynamical systems, that involves perturbing around high-order singularities to map the bifurcation landscape. In this paper singularity theory is used as a diagnostic tool to probe the relationship between the bifurcation structure of dynamical models for and the physics of confinement transitions. We study the stability of solutions, interrogate degenerate or pathological singularities, and compute and present key bifurcation diagrams.

The bifurcation structure of Eqs 10–12 predicts behaviours observed repeatably in magnetic fusion experiments, such as shear flow suppresion of turbulence, and hysteretic, non-hysteretic, and oscillatory transitions.[16,17] However, there are several outstanding issues that suggest the model is still incomplete. This section can be read therefore as a sequel to refs. 16 and 17 in which (unlike most sequels) the most interesting parts of the story are told.

The first issue is a trapped degenerate singularity, revealed by inquisitive review of the bifurcation structure of Eqs 10–12. It is responsible for an unphysical prediction of the model: that the shear flow increases without bound as the power input is withdrawn. The second issue is the thermal diffusivity term that was neglected in the derivation in section 3. It turns out to have profound effects on the bifurcation structure. The third concerns the strand (2) view of confinement transitions. I propose a unified model in which this physics is included as a direct conversion channel between gradient potential energy and shear flow kinetic energy.

4.1. *The case of the trapped singularity*

A bifurcation diagram of the equilibria (or steady states) of Eqs 10–12 is displayed in Fig. 4(a), rendered for all three variables v', P, and N, with the power input Q as the control parameter. Stable and unstable equilibria are marked with solid and dashed lines respectively, and amplitude envelopes of enclaves of periodic solutions, which begin to occur at Hopf bifurcations on the equilibrium curves, are marked by large black dots.* Note that P and N, being quadratic energy variables, have a positive domain only, while the shear flow v', as a velocity variable, may be positive or negative. In the P and N renderings, therefore, solution curves are annotated to distinguish between energies that correspond to the $+v'$ and $-v'$ domains. The distinction is important: if we are interested, for example, in knowing the turbulent kinetic energy N that results from evolving this system to the $-v'$ branch in (a), the naïve use of the $+v'$ value of N gives an underestimate. I highlight two other interesting features that have particular relevance to this discussion.

(1) On the $-v'$ branch if the power input ebbs below the turning point labeled s0 the shear flow must *spontaneously* reverse direction to the $+v'$ domain. The zoom-in shows a small range of Q over which there are five steady state solutions, or fivefold multiplicity, comprising three stable and two unstable branch segments. Other kinds of fivefold multiplicity also occur in this system which are qualitatively different from this and from each other. They will be shown later. In the remainder of this discussion I ignore the $-v'$ domain.

(2) Considering the branch of *unstable* solutions occurring in the top left-hand corner of the v' and P renderings, and in the lower left-hand corner of the N rendering, leads us to the crucial issue of unbounded shear flow growth. For $\varphi = 0$ this branch is nonexistent, but because we are

*The bifurcation diagrams in this work were computed numerically using the continuation code AUTO, http://indy.cs.concordia.ca/auto/. Given a starting equilibrium, AUTO continues the solutions as a function of the selected bifurcation parameter, computes the eigenvalues at each step (and therefore the stability), flags bifurcation points, where it can continue solution branches in a second parameter, and computes the amplitude, period, and stability (using Floquet exponents) of periodic solutions.

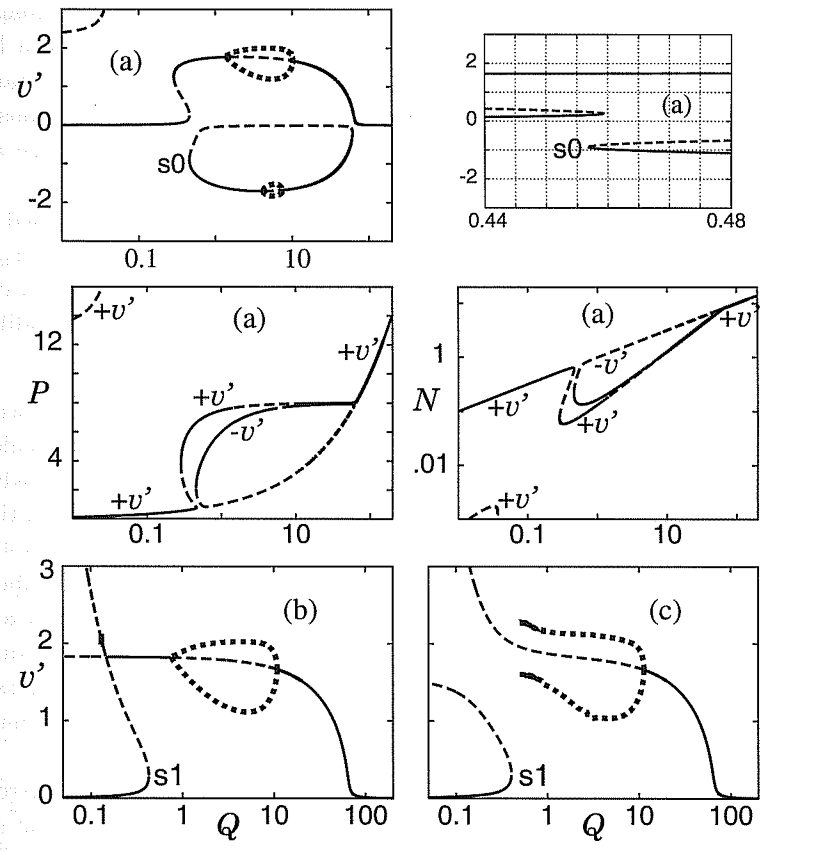

Fig. 4. (a) $\varphi = 0.05$. For clarity in the N and P renderings the limit cycle envelopes are not shown and the solution curves are annotated to indicate whether they correspond to the $+v'$ or $-v'$ domain. (b) $\varphi \approx 0.08059 = \varphi_{Tm}$. (c) $\varphi = 0.11$. Other parameters: $\beta = 1$, $\gamma = 1$, $\alpha = 2.4$, $b = 1$, $a = 0.3$, $\varepsilon = 1.5$.

smoothly increasing φ from zero it is more illuminating to consider the branch as representing the interaction of φ with the nonlinear viscosity term in Eq. 12. From this point of view the branch is trapped as a singularity — a turning point — at $(v', Q) = (\infty, 0)$ for $\varphi = 0$. As φ is increased smoothly from zero the "new" branch, retaining the turning point, is released from its trap and begins to interact with the "old" branches and at φ_{Tm} the new and old branches exchange arms, (b). Singularity theory describes φ_{Tm} as an *organizing centre*, a loose but useful and evocative name for the highest order singularity in some maximum in v' is created because s4 formally is a turning point. At the given values of the other parameters an islet of steady-state solutions is formed, but the bifurcation diagram should be visualized as a slice of a surface where the third coordinate is a second parameter of the system. Two slices of this surface are shown in Fig. 5(c) and (d) where the other turning points are labeled s1, s2, and s3. From the low shear flow solution branch we make the forward transition at s1 and progress through the onset of an oscillatory regime, as in Fig. 4. This segment is henceforth designated as the *intermediate* shear flow branch, and the islet or peninsula as the *high* shear flow branch. In (c) a back-transition to the low shear flow state (it is actually not zero) occurs at s2. The islet can only be reached via a transient. In (d) we see a radical difference in the global dynamics: with **diminishing** Q the shear flow **grows**, passes through a second oscillatory regime, reaches the maximum then falls steeply, and **the back-transition at s4 occurs at relatively low power input**.

4.3. *Thermal diffusivity is not negligible*

The next step is to modify Eq. 10 to include a linear thermal energy sink:

$$\varepsilon\frac{\mathrm{d}P}{\mathrm{d}t} = Q - \gamma NP - \chi P, \tag{15}$$

where χ is a lumped dimensionless parameter that represents cross-field thermal diffusivity[18] and other non-turbulent or residual losses.[19] The model now consists of Eqs 13, 14, and 15, and the corresponding energy flux schematic is Fig. 3(c). Figure 6 shows a series of bifurcation diagrams computed for increasing values of χ.

A qualitative change from Fig. 5(d) is immediately apparent — two new turning points s5 and s6 have appeared in (a). They were born from a local cusp singularity but the global effect is to stoop and shift the entire pensinsular towards higher Q. As in Fig. 5, the system transits to an intermediate shear flow state at s1, but from this branch the effect of decreasing Q is radically different: at s6 *another discontinuous transition* occurs to a high shear flow state on the peninsula. In (b) between s5 and s6 there is a range of fivefold multiplicity, which in (c) has disappeared in a surprisingly mundane way: not through a singularity but merely by the shift of the peninsula toward higher Q. But the shift creates a new and qualitatively different range of fivefold multiplicity through the creation of s7 and s8 at another cusp singularity. In (d) s4 and s7 have been annihilated at yet another cusp. Thus there are four cusps, the origins of which can be seen

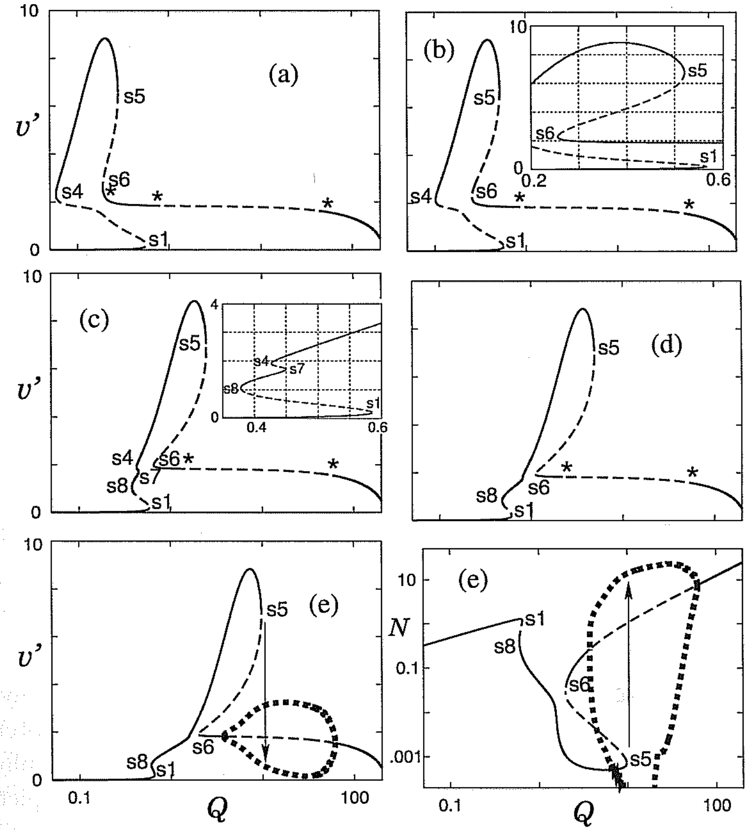

Fig. 6. (a) $\chi = 0.005$, (b) $\chi = 0.01$, (c) $\chi = 0.05$, (d) $\chi = 0.1$, (e) $\chi = 0.2$. Other parameters: $\kappa = 0.001$, $\varphi = 0.088$, $\beta = 0.3$, $\alpha = 2.4$, $b = 1$, $a = 0.3$, $\gamma = 1$, $\varepsilon = 1$.

in the 2-parameter diagram of Fig. 7, onto which the lines of s1, s4, s5, s6, s7, and s8 over χ are projected. From the high shear flow branch in Fig. 6(c), (d), and (e), increasing Q induces the system to transit at s5 to a limit cycle rather than to a steady state on the intermediate branch. In (e) we see super-suppression of the turbulence N corresponding to this enormous uptake of energy by the shear flow, but the hard onset of oscillations with the transition at s5 causes the turbulence to rise again dramatically, with other parameters as given.

Note that the Hopf bifurcation that is starred near s6 in (a) has vanished in (b)–(e). It coalesces with s6 at a degenerate point characterized by one real zero and a pair of purely imaginary complex conjugate eigenval-

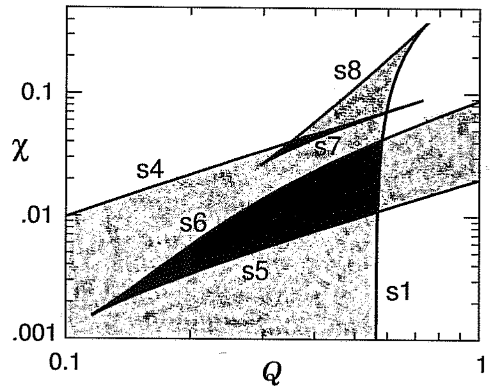

Fig. 7. In the two black areas there are five steady states and in the dusted areas there are three steady states.

ues, known as a saddle-node Hopf (SNH) bifurcation. Evidently the SNH bifurcation occurs between $0.005 < \chi < 0.01$.

4.4. *Strands (1) and (2) are unified*

Finally I address the strand (2) view of confinement transition physics. The published models for this process have no coupling to the potential energy and turbulence dynamics. Here, in contrast, the ion orbit loss physics associated with edge electric fields is included as a piece of a holistic picture, so that the model now consists of Eq. 13 and

$$\varepsilon\frac{\mathrm{d}P}{\mathrm{d}t} = Q - \gamma NP - v'^2 r(P) - \chi P \tag{16}$$

$$2\frac{\mathrm{d}v'}{\mathrm{d}t} = \alpha v' N - \mu(P,N)v' + v' r(P) - \kappa v' + \varphi. \tag{17}$$

The new term $r(P) = \nu \exp\left[-\left(w^2/P\right)^2\right]$ simply says that the rate at which ions are lost, and flow generated, is proportional to a collision frequency ν times the fraction of collisions that give ions sufficient energy to escape. The energy factor assumes a Maxwellian ion distribution and w^2 is proportional to the square of the critical escape velocity. This is the simplified essence of expressions used by earlier authors,[6,7] except that I have included explicitly the temperature dependence of r through P. The corresponding energy schematic is Fig. 3(d) where it is seen that $r(P)$ is a competing potential energy conversion channel that can dominate the dynamics when the critical escape velocity w is low or the pressure is high.

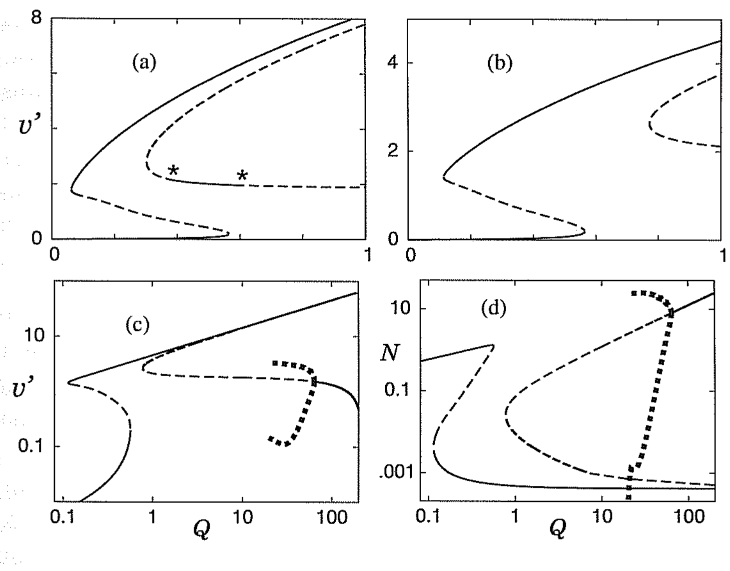

Fig. 8. (a) $\nu = 0.015$, (b), (c), and (d) $\nu = 0.05$. Other parameters: $\chi = 0.01$, $\kappa = 0.001$, $\varphi = 0.088$, $\beta = 0.3$, $\gamma = 1$, $\alpha = 2.4$, $b = 1$, $a = 0.3$, $w = 1$, $\varepsilon = 1$.

This is exactly what we see in the bifurcation diagrams, Fig. 8. The high shear flow peninsula is elongated and flattened. The Hopf bifurcations in (a), where $r(P)$ is small, have disappeared in (b) through a DZE, leaving the intermediate branch unstable until the remaining Hopf bifurcation (c) is encountered. In the transition region the bifurcation diagram begins to look more like the simple S-shaped, cubic normal form schematics featured in numerous papers by earlier authors.[6,7] However, this **unified** model accounts for shear flow suppression of the turbulence (d), whereas theirs could not.

5. Discussion

In summary, the strands (1) and (2) physics of plasma confinement transitions are smoothly unified for the first time in a physics-based, predictive dynamical model, analysis of which distils the global dynamics of the system. With incorporation of a simple term for downscale energy flux, allowing effective small scale dissipation independent of the temperature, when the direct shear flow drive φ is high enough to join the islet to the peninsula, the shear flow can rise as the power input ebbs. There is concomitant super-suppression of turbulence and a back-transition at very low power input.

A report in,[20] where a parameter equivalent to φ was used as the control parameter, supports the super-suppression of turbulence found here. Non-turbulent dissipation introduces the capacity for discontinuous transitions to a super-suppressed turbulence regime, but oscillations may onset. These results suggest new and interesting—and potentially cost-saving in terms of heating power—strategies for controling confinement in fusion experiments.

Appendix A. Singularity theory

A non-technical reference on singularity theory that is accessible to the physics reader is Ball,[9] which also gives other key references on the mathematics and physical applications. Systematic bifurcation, singularity, and stability analysis provide *qualitative* information on the global behaviour of a dynamical system†, in the following sense:

In attempting to understand the behavior of a complex system with many degrees of freedom a standard approach is to begin by making a simplified model of the process — a dynamical system — and within the confines of that model analyse what it has to tell us about the process. Yet very few dynamical systems have known, exact solutions. For the vast majority it cannot even be proved that general solutions exist. Qualitative methods, pioneered by Poincaré in his work on the restricted three-body problem, can tell us how solutions *would* behave, assuming they *do* exist, as parameters are varied.

For an experimental or real-world macroscopic dynamical system we are often interested in questions that qualitative analysis can answer, rather than numerical solutions. Is it capable of discontinuous, periodic, or chaotic dynamics? Can we draw the bounds of this behaviour in parameter space, so that we may design or manage experiments to include, forbid, or modify such action? We can also use qualitative analysis to improve the model itself. In the following section these capabilities of singularity theory are illustrated using the model described by Eqs 10–12.

Persistent, degenerate singularities inform us about physics:

For a dynamical system

$$\frac{\mathrm{d}\mathbf{x}}{\mathrm{d}t} = \mathcal{F}(\mathbf{x}, \lambda_1, \cdots \lambda_n)$$

†This means the behaviour over the $m + n$-dimensional space of m dynamical state variables and n independent parameters.

where the components of $\mathbf{x}$ are dynamical state variables and the λ_i are parameters, the equilibria are found by setting the right hand sides to zero and solving to obtain a single algebraic equation in terms of one of the state variables x:

$$G(x, \lambda_1, \cdots \lambda_n) = 0. \tag{A.2}$$

The function $G(x, \lambda_1, \cdots \lambda_n)$ is called the *bifurcation problem.* Solutions of (A.2) that also satisfy the additional condition

$$G_x = 0, \tag{A.3}$$

where the subscript notation denotes partial differentiation with respect to x, are called *singular* points or singularities. Points where conditions (A.2) and (A.3) hold and, in addition, one or more higher order partial derivatives is zero are known as *degenerate* or *higher order* singularities.

An example of a degenerate singularity that has physical importance in the current context is the pitchfork, for which the defining and non-degeneracy conditions are

$$G = G_x = G_{xx} = G_{\lambda_1} = 0, \; G_{xxx} \neq 0, \; G_{x\lambda} \neq 0. \tag{A.4}$$

Applying these conditions to Eqs 10–12 we find, with the aid of some computer algebra, the unique pitchfork $\mathbf{P}$ at

$$(v', Q, \beta, \varphi) = \left(0, \frac{\alpha^2\gamma^2}{9a^2b}, \frac{2\alpha^3\gamma\sqrt{\alpha/a}}{27\sqrt{3}\,a^2b}, 0\right). \tag{P}$$

At $\mathbf{P}$ the two non-degeneracy conditions in Eq. A.4 evaluate as $g_{PQ} = 8a/\alpha$, $g_{PPP} = -18a\gamma^2/(\alpha\beta)$. We see that the pitchfork is a twice-degenerate, or codimension 2, singularity because two parameters in addition to the principal bifurcation parameter Q are required to define it. The bifurcation diagram for the equilibria of Eqs 10–12 at the critical values of the dissipative parameter β and and the symmetry-breaking parameter φ is shown in in Fig. A1(a). In (b) and (c) β is relaxed either side of the critical value, but φ is held at zero.

The other singularity $\mathbf{T}$ on $v' = 0$ in Fig. A1 satisfies the defining and non-degeneracy conditions for a transcritical bifurcation,

$$G = G_x = G_{\lambda_1} = 0, \; G_{xx} \neq 0,$$

$$\det \begin{pmatrix} G_{xx} & G_{\lambda_1 x} \\ G_{x\lambda_1} & G_{\lambda_1\lambda_1} \end{pmatrix} \equiv \det d^2G < 0. \tag{A.5}$$

It is once-degenerate but also requires the symmetry-breaking parameter for full determination.

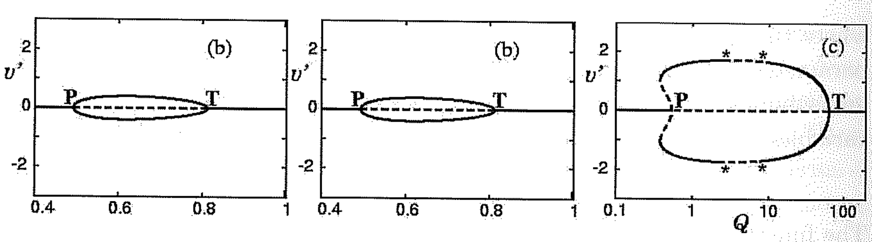

Fig. A1. Bifurcation diagrams showing the fully degenerate (a) and partially unfolded (b) and (c) pitchfork **P**. (a) $\beta = \beta_{crit} \approx 18.58$, (b) $\beta = 50$, (c) $\beta = 1$. Other parameters: $\varphi = 0$, $\gamma = 1$, $b = 1$, $a = 0.3$, $\alpha = 2.4$, $\varepsilon = 1.5$.

We see from Fig. A1 that the pitchfork is persistent to variations in β. (In fact it is persistent to variations in all parameters of Eqs 10–12 other than φ. Persistence of a degenerate singularity when there are not enough independent parameters to unfold it was not recognized in some previous models for confinement transitions, where such points were wrongly claimed to represent second-order phase transitions.) Furthermore, as long as the degenerate singularity **P** persists the model cannot be predictive near it. This may be viewed as an overdetermination problem: with φ fixed at zero we see from (A.4) there are four defining conditions but we have only three variable quantities, v', Q, and β.

Typically the pitchfork is associated with a fragile symmetry in the physics of the modelled system. In this case the symmetry is obvious from Fig. A1: in principle the shear flow can be in either direction equally. In real life (or *in numero*), experiments are always subject to perturbations that determine a preferred direction for the shear flow (such as friction with neutrals, or any other asymmetric shear-inducing mechanism), and the pitchfork is inevitably dissolved, or unfolded. In the bifurcation diagrams of Figs 4, 5, 6, and 8 the pitchfork in Fig. A1 is fully unfolded, giving us a more realistic picture of confinement transition dynamics.

More generally, in analysing a dynamical model we are interested in the mapping between the bifurcation and stability structure and the physics of the process the model is supposed to represent. If we probe this relationship we find that degenerate singularities correspond to some essential physics (such as fulfilling a symmetry-breaking imperative, or the onset of hysteresis, or resolving an "infrared catastrophe" type of anomaly), or they are pathological. In the first case we can usually unfold the singularity in a physically meaningful way; in the other case we know that something is amiss and we should revise our assumptions.

Definitions of symbols, notation, and approximations.

$\mathbf{v} = \frac{1}{B_0}\hat{\mathbf{z}} \times \nabla\phi = \mathbf{v}_0 + \tilde{\mathbf{v}}$	$\mathbf{E} \times \mathbf{B}$ flow velocity
$\mathbf{v}_0 = \langle \mathbf{v} \rangle$	average background component
$\tilde{\mathbf{v}}$	fluctuating or turbulent component
$p = p_0 + \tilde{p}$	plasma pressure
$p_0 = \langle p \rangle$	average background component
$\tilde{p}$	fluctuating or turbulent component
B_0	magnetic field along the z axis
ρ	average mass density of ions, constant
μ	ion viscosity coefficient
η	resistivity
ν	frictional damping coefficient
$\Omega' \equiv \mathrm{d}\Omega/\mathrm{d}x > 0$	average field line curvature, constant
$\nabla_\perp^2$	$\partial_x^2 + \partial_y^2$
χ	cross-field thermal diffusivity coefficient
V	external flow
$p_0(x) \simeq p_{0_{(x=\delta)}} + x\mathrm{d}p_0/\mathrm{d}x \equiv x\mathrm{d}p_0/\mathrm{d}x$	†
$v_0(x) \simeq v_{0_{(x=\delta)}} + x\mathrm{d}v_0/\mathrm{d}x \equiv x\mathrm{d}v_0/\mathrm{d}x$	†
$v' = \pm\sqrt{F}$	poloidal shear flow
$E_p \equiv Q =$ constant	power input to the pressure gradient
$E_N \simeq \gamma/PN$	turbulence growth rate
$E_F \simeq \alpha FN$	transfer rate due to the Reynolds stress
$\epsilon_N \simeq \beta N^2$	turbulent energy dissipation rate
$\epsilon_F \simeq \mu(P,N)F$	damping rate due to viscosity
$\mu(P,N) = bP^{-3/2} + aPN$	neoclassical and turbulent viscosities
$E_\varphi \simeq \varphi F^{1/2}$	shear flow driving rate
$\varphi \simeq \delta\nu V$	

†The constant terms $p_{0_{(x=\delta)}}$ and $v_{0_{(x=\delta)}}$ are dropped in the definitions of $p_0(x)$ and $v_0(x)$.

Acknowledgments

This work is supported by the Australian Research Council.

References

1. E. S. Oran and V. N. Gamezo, Origins of DDT in gas-phase combustion. Preprint, NRL Laboratory for Computational Physics and Fluid Dynamics, Washington DC, 2006.
2. R. H. Kraichnan and D. Montgomery, Two-dimensional turbulence. *Reports on Progress in Physics*, **43**, 547–619 (1980).
3. P. W. Terry, Suppression of turbulence and transport by sheared flow. *Reviews of Modern Physics*, **72**(1), 109–165 (2000).

4. P. H. Diamond and Y.-B. Kim, Theory of mean poloidal flow generation by turbulence. *Physics of Fluids B*, **3**, 1626–1633 (1991).
5. E-J. Kim, P. H. Diamond, and T. S. Hahm, Transport reduction by shear flows in dynamical models. *Physics of Plasmas*, **11**(10), 4554–4558 (2004).
6. S.-I. Itoh and K. Itoh, Model of *L*- to *H*-mode transition in tokamak. *Physical Review Letters*, **60**(22), 2276–2279 (1988).
7. K.C. Shaing and E.C. Jr Crume, Bifurcation theory of poloidal rotation in tokamaks: a model for the L–H transition. *Physical Review Letters*, **63**(21), 2369–2372 (1989).
8. S Magni, C. Riccardi, and H. E. Roman, Statistical investigation of transport barrier effects produced by biasing in a nonfusion magnetoplasma. *Physics of Plasmas*, **11**(10), 4564–4572 (2004).
9. R. Ball, Singularity theory. In Alwyn Scott, editor, *Encyclopedia of Nonlinear Science*, New York, 2005. Routledge.
10. R. Ball and R. L. Dewar, Singularity theory study of overdetermination in models for L–H transitions. *Physical Review Letters*, **84**(14), 3077–3080 (2000).
11. H. R. Strauss, Dynamics of high β tokamaks. *The Physics of Fluids*, **20**(8), 1354–1360 (1977).
12. B. A. Carreras, L. Garcia, and P. H. Diamond, Theory of resistive pressure-gradient-driven turbulence. *Physics of Fluids*, **30**(5), 1388–1400 (1987).
13. H. Sugama and M. Wakatani, A transport study for resistive interchange mode turbulence based on a renormalized theory. *J. Phys. Soc. Japan*, **57**(6), 2010–2025 (1988).
14. H. Sugama and W. Horton, Shear flow generation by Reynolds stress and suppression of resistive *g* modes. *Physics of Plasmas*, **1**(2), 345–355 (1994).
15. H. Sugama and W. Horton, Transport suppression by shear flow generation in multihelicity resistive-*g* turbulence. *Physics of Plasmas*, **1**(7), 2220–2228 (1994).
16. R. Ball, R. L. Dewar, and H. Sugama, Metamorphosis of plasma shear flow–turbulence dynamics through a transcritical bifurcation. *Physical Review E*, **66**, 066408–1–066408–9 (2002).
17. R. Ball, Suppression of turbulence at low power input in a model for plasma confinement transitions. *Physics of Plasmas*, **12**, 090904–1–8 (2005).
18. S. I. Braginskii, Transport processes in a plasma. In M. A. Leontovich, editor, *Reviews of Plasma Physics*, volume 1. Consultants Bureau, New York, 1965.
19. A. Thyagaraja, F. A. Haas, and D. J. Harvey, A nonlinear dynamical model of relaxation oscillations in tokamaks. *Physics of Plasmas*, **6**(6), 2380–2392 (1999).
20. Y. and Kishimoto, *Plasma Physics and Controlled Nuclear Fusion Research (IAEA-CN-60/D-10, Vienna*, **3**, 299 (1994).

ZONAL FLOW GENERATION BY MODULATIONAL INSTABILITY

ROBERT L. DEWAR AND R. F. ABDULLATIF

Department of Theoretical Physics,
Research School of Physical Sciences and Engineering,
The Australian National University,
Canberra ACT 0200, Australia
robert.dewar@anu.edu.au

This paper gives a pedagogic review of the envelope formalism for excitation of zonal flows by nonlinear interactions of plasma drift waves or Rossby waves, described equivalently by the Hasegawa–Mima (HM) equation or the quasi-geostrophic barotropic potential vorticity equation, respectively. In the plasma case a modified form of the HM equation, which takes into account suppression of the magnetic-surface-averaged electron density response by a small amount of rotational transform, is also analyzed. Excitation of zonal mean flow by a modulated wave train is particularly strong in the modified HM case. A local dispersion relation for a coherent wave train is calculated by linearizing about a background mean flow and used to find the nonlinear frequency shift by inserting the nonlinearly excited mean flow. Using the generic nonlinear Schrödinger equation about a uniform carrier wave, the criterion for instability of small modulations of the wave train is found, as is the maximum growth rate and phase velocity of the modulations and zonal flows, in both the modified and unmodified cases.

1. Introduction

As of January 1, 2006, Wikipedia[1] introduces the term "zonal flow" thus:

> Fluid flow is often decomposed into mean and deviation from the mean, where the averaging can be done in either space or time, thus the mean flow is the field of means for all individual grid points. In the atmospheric sciences, the mean flow is taken to be the purely *zonal flow* of the atmosphere which is driven by the temperature contrast between equator and the poles.
> In geography, geophysics, and meteorology, *zonal* usually means 'along a latitude circle', i.e. 'in the east-west direction'. In atmospheric sciences the zonal coordinate is denoted by x, and the zonal wind speed by u.